# CMS Physics Analysis Summary

Contact: cms-pag-conveners-b2g@cern.ch 2013/11/18

# Search for Vector-Like b′ Pair Production with Multilepton Final States in pp collisions at $\sqrt{s} = 8$ TeV

The CMS Collaboration

## Abstract

A search for pair-production of vector-like partners of the b quark, b′, is carried out in events with at least three leptons using 19.5 fb$^{-1}$ of integrated luminosity in pp collisions at $\sqrt{s} = 8$ TeV collected by the CMS experiment at the LHC. The data are binned in multiple exclusive channels according to the amount of expected standard model background in order to increase the search sensitivity. The observations are consistent with the standard model expectations. The search is interpreted for different b′ masses and for varying branching ratios to the bZ, tW, and bH states. We exclude b′ quarks with masses less than values in the range of 520−785 GeV (depending on the values of the branching ratios) at the 95% confidence level.

# 1 Introduction

We present a search for b′, which is a vector-like partner of the b quark. "Vector-like" fermion in this context means that the left- and right-handed chiralities transform in the same fashion under the SM gauge group $SU(3)_C \otimes SU(2)_L \otimes U(1)_Y$. Just as new physics such as supersymmetry could stabilize the mass of the Higgs boson, recently discovered at the LHC [1, 2], partner quarks to the third generation quarks can also serve this purpose. In Little Higgs models [3, 4] these partner quarks cancel the loop contributions from the top quark to the Higgs boson mass. For such a cancellation to be effective, the mass of the partner quarks should be of the same order of magnitude as that of the top quark, i.e. below a TeV.

The partner quarks can be introduced as a straightforward fourth generation extension to the standard model (SM) [2]. However, a sequential fourth generation of this nature is disfavored because the enhancement of the couplings in the $H \to \tau\tau$ and $H \to \gamma\gamma$ channels is incompatible with recent measurements [5]. Vector-like partner quarks [6], on the other hand, are unaffected by this constraint and are still viable candidates for canceling the quadratic divergences in the Higgs mass. These partner quarks are thus an attractive alternative to supersymmetry for the solution of the hierarchy problem.

We present here a search for the pair production of the b′ partner quark in 8 TeV pp collisions in which three or more leptons are produced. The decay mode that is expected to be dominant for the b′ is to a top quark and a W boson (i.e. $b' \to tW$). However, we keep this search for new physics general by also considering flavor-changing neutral current (FCNC) decays to a bottom quark with a Z boson (i.e. $b' \to bZ$) or to a bottom quark with a SM Higgs boson (i.e. $b' \to bH$). The latter could potentially be the more significant of the two FCNC decay modes [7]. We consider the branching ratios to the three modes to be arbitrary, but subject to the constraint that they add to unity. We do not consider other decay modes of the b′. Since a b′ quark can potentially decay in three different modes, there are six distinct event types for pair-produced b′ quarks: bZbZ; tWtW; bHbH; bZtW; bZbH; and tWbH. After taking into account the top decay to bW, the possible decay modes are bbZZ, bbWWWW, bbHH, bbWWZ, bbZH and bbWWH. We assume the SM Higgs boson to have a mass of 125 GeV and obtain its branching ratios from [8].

# 2 Data samples and event selection

The data sample used in this analysis corresponds to an integrated luminosity of 19.5 $fb^{-1}$ recorded in 2012 with the CMS detector at the LHC. The CMS detector has cylindrical symmetry around the pp beam axis with tracking and muon detector pseudorapidity coverage to $|\eta| < 2.4$, where $\eta = -\ln\tan(\theta/2)$ and $\theta$ is the polar angle with respect to the counterclockwise beam. The azimuthal angle $\phi$ is measured in the plane perpendicular to the beam direction. The data used for the search were collected using double-lepton triggers (double-electron, double-muon and electron-muon). The transverse momentum ($p_T$) lower thresholds for these triggers are 17 GeV for the lepton with highest $p_T$ and 8 GeV for the lepton with second highest $p_T$. The trigger efficiencies are measured directly using a data sample independently triggered by $H_T$, defined as the scalar sum of the transverse momentum of all jets with $p_T > 40$ GeV, assuming no correlations between this and the signal triggers.

The double-muon trigger efficiency is measured to be 90% with no significant $p_T$ dependence. For events with a second lepton with $p_T > 20$ GeV, the double-electron trigger efficiency is 95%, while that of the muon-electron trigger is 93%. For events with a second lepton with

$p_T < 20$ GeV, the double-electron trigger efficiency is 82%, while the electron-muon trigger efficiency is 86%. We weight each simulated event by the probability for it to satisfy the double-lepton triggers. The uncertainty in the correction to the simulation translates into a systematic uncertainty in the irreducible backgrounds and signal efficiencies.

All detector simulations are performed using GEANT4 [9]. The important SM backgrounds for this analysis ($t\bar{t}$ pair production, double vector-boson production, and rare processes with vector bosons and top quarks) were generated using MADGRAPH 5 v1.4.4 [10, 11]. We use the CTEQ6L1 parton distribution functions for all processes [12]. For the dominant VV+jets contribution, up to two jets were selected at the matrix element level in MADGRAPH. Cross sections for the signal processes are calculated using the Top++2.0 software [13]. We use simulated events for the purpose of estimating signal acceptance and for determining SM background contribution when they can not be estimated using data alone.

## 3 Object reconstruction

This analysis requires the presence of at least three reconstructed lepton candidates. The allowed candidates include electrons, muons, and hadronically-decaying taus; taus decaying leptonically are included in the electron and muon categories. We use electrons and muons with $p_T > 10$ GeV and $|\eta| < 2.4$. They are reconstructed using measured quantities from the tracker, calorimeter, and muon system using the particle flow (PF) algorithm [14]. The matching candidate tracks must satisfy quality requirements and spatially match with the energy deposits in the electromagnetic calorimeter or the tracks in the muon detectors, as appropriate. Details of reconstruction and identification can be found in [15] for muons and in [16] for electrons.

We consider hadronic tau decays which yield either a single charged track (one-prong) or three charged tracks (three-prong) with or without additional electromagnetic energy from neutral pion decays. The hadronic tau candidates are reconstructed using the hadron plus strips (HPS) PF algorithm [17], which reconstructs the various hadronic decay modes and rejects candidates that appear to be poorly reconstructed electrons and muons. We require tau candidates to have $p_T \geq 20$ GeV and $|\eta| < 2.3$.

An isolation requirement strongly reduces the SM background from misidentified leptons. We define the relative isolation $I_{rel}$ as the ratio of the sum of the calorimeter energy, using the PF algorithm, and the $p_T$ of any other tracks in a cone defined by $\Delta R = \sqrt{(\Delta\eta)^2 + (\Delta\phi)^2} < 0.3$ around the lepton to the $p_T$ of the lepton. The sum of energy in the isolation cone is corrected by subtracting out the contributions from charged particles from additional collisions in the event. For electrons and muons, we require $I_{rel} < 0.15$. For the absolute isolation $I$ of the hadronic tau decays we require that the sum of the energy in a cone radius of 0.5 in $\Delta R$ around a tau candidate be less than 2 GeV after excluding the expected contribution from additional overlapping pp interactions in the same or preceding bunch crossing (pile-up).

After the isolation requirement on the leptons is imposed, the most significant background sources are residual non-prompt leptons from heavy quark decays. These leptons have a higher probability of being isolated because of their larger momentum with respect to the jet axis, which can be misidentified as prompt leptons. This background is reduced by requiring that the leptons originate from within 0.5 cm of the primary vertex in the $z$ direction, and that the impact parameter $d_0$ between the track and the event vertex in the plane transverse to the beam axis be small: $|d_0| \leq 0.02$ cm. This ensures that the muons and electrons are consistent with

being produced directly at the primary vertex.

Jets are reconstructed from PF objects using the anti-$k_T$ algorithm [18] with a distance parameter of 0.5. Jet energy scale corrections obtained from data and MC simulation are applied to account for the nonlinear response of the calorimeter and pileup effects [19, 20]. We classify events according to the absence or presence of one or more b jets. The CMS Combined Secondary Vertex algorithm [21] is used to identify jets that are consistent with having originated from the hadronization of b quarks. The working point is chosen such that we obtain a b-tagging efficiency of 70%, a c-tagging efficiency of 10-20%, and a misidentification rate for light flavor jets of 1%.

The missing transverse energy, $E_T^{miss}$, is defined as the magnitude of the transverse component of the vectorial sum of the momenta of all particle candidates. Comparisons between data and simulation show good modeling of $E_T^{miss}$ for processes with genuine $E_T^{miss}$ from neutrinos [22, 23].

## 4 Search strategy

Multilepton events are classified on the basis of the number of leptons, lepton and jet flavor, charge and flavor combinations, and other kinematic quantities described below. To maintain high sensitivity, the search channels with hadronic tau candidates are separated from electron and muon channels due to the larger backgrounds arising from the higher tau misidentification rate.

We classify each event in terms of the maximum number of opposite-sign same flavor (OSSF) dilepton pairs that can be made by using each identified electron or muon candidate only once. For example, both $\mu^+\mu^-\mu^-$ and $\mu^+\mu^-e^-$ have one OSSF pair, denoted by OSSF1; $\mu^+\mu^+e^-$ has no OSSF pairs, denoted by OSSF0; and $\mu^+\mu^-e^+e^-$ has two OSSF pairs, denoted by OSSF2. We denote a lepton pair of different flavors as $\ell\ell'$, where $\ell$ indicates an electron or a muon. The level of SM background varies considerably across the channels. Channels with hadronic tau decays or containing OSSF pairs suffer from larger backgrounds compared to channels with OSSF0.

We further classify events as containing a leptonically-decaying Z if at least one OSSF pair has a reconstructed invariant mass, $m(\ell^+\ell^-)$, inside the Z-mass window (75-105 GeV), referred to as on-Z. Events with $m(\ell^+\ell^-)$ outside the Z-mass window are denoted as off-Z. We reject events with $m(\ell^+\ell^-) < 12$ GeV to discard events from low mass Drell Yan processes and low mass resonances such as $J/\psi$ and Y. In order to remove lepton conversions that arise from final state radiation in Z boson decay products, we reject events where $|m(\ell^+\ell^-) - m_Z| > 15$ GeV but $|m(\ell^+\ell^-\ell'^{\pm}) - m_Z| < 15$ GeV or $|m(\ell^+\ell^-\ell^{\pm}) - m_Z| < 15$ GeV, but only if the event has low-$E_T^{miss}$ and low-$H_T$, such as in the case of Z+jet production.

The SM background can be further reduced by requirements on either hadronic activity or missing energy. The presence of hadronic activity in an event is characterized by the variable $H_T$, defined as the scalar sum of the transverse momentum of all jets with $p_T > 30$ GeV and $|\eta| < 2.5$. Jets used for the $H_T$ determination must be well separated from any identified lepton and this is enforced by requiring that there are no isolated leptons present in a cone of $\Delta R < 0.3$ around the jet axis.

We define $S_T$ as the scalar sum of $E_T^{miss}$, $H_T$, and the $p_T$ of all isolated leptons. $S_T$ is a useful quantity in this search because its distribution peaks near the sum of the parent particle masses

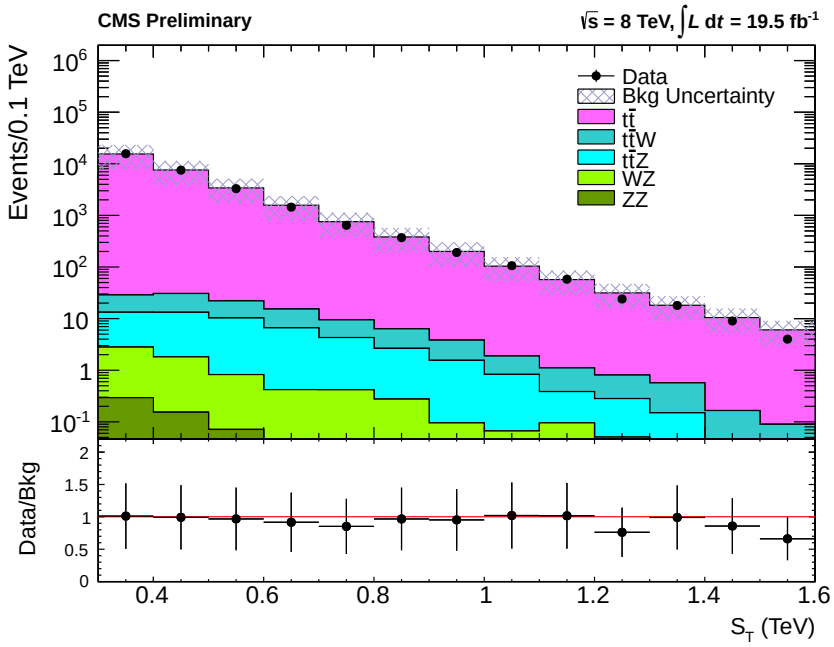


Figure 1: The $S_T$ distribution in an opposite sign e-$\mu$ $t\bar{t}$ control region. The uncertainties in the ratio plot below include both statistical and systematic uncertainties.

if most of the energy is reconstructed as leptons, jets or $E_T^{miss}$. Therefore, events containing the production and decay of heavy particles, such as the signal events in this analysis, are expected to have much larger $S_T$ than SM backgrounds. We divide the $S_T$ distribution into several bins: 0-0.3; 0.3-0.6; 0.6-1.0; 1.0-1.5; 1.5-2.0; and above 2.0 TeV. The $S_T$ binning is designed to have the ZZ and WZ backgrounds in the lowest bin and $t\bar{t}$ straddling the lowest two bins, thus leaving the signal to occupy higher bins with relatively small background.

# 5 Backgrounds

The main SM background sources in this search are dilepton processes such as Z+jets when accompanied by a third non-prompt lepton that passes selection criteria, WZ production leading to three leptons, $t\bar{t}$ production followed by leptonic decays of the W bosons and finally when an off-shell photon in a process with two or more leptons undergoes an asymmetric conversion leading to another reconstructed lepton. The backgrounds listed above are estimated with both data-driven and simulation-based techniques as described in the following sections.

## 5.1 Background from $t\bar{t}$ production

The background from $t\bar{t}$ production is estimated from simulation after validation in single lepton and dilepton control regions enriched with this process. The single lepton control region requires exactly one isolated muon with $p_T > 30\,\text{GeV}$, at least 3 jets, one of which must be tagged as a b jet, and $S_T > 300\,\text{GeV}$. It is used to study the relative isolation distribution of non-prompt leptons from jets. The dilepton control region requires an e$\mu$ pair and is used to compare kinematic variables like $S_T$ (see Figure 1), $H_T$ and $E_T^{miss}$ between data and simulation. In addition, the distribution of the number of jets is reweighted to match the data in the dilepton control region. The same reweighting is applied to the signal region.

## 5.2 Background from non-prompt leptons or tau candidates

We use data to estimate background contributions from processes with two genuine leptons and one or more misidentified leptons such as $Z(\to 2\ell) + \text{jets}$ and $W^+W^-(\to 2\ell + E_T^{miss}) + \text{jets}$. This is because the QCD component of the simulation cannot be assumed to be reliable in a rare situation when fragmentation fluctuations lead to the jet being misidentified as a lepton.

To estimate this background, we use data with two reconstructed leptons and an additional isolated track scaled by an extrapolation factor between isolated tracks and lepton candidates from jets. This extrapolation factor is measured in control samples where no signal is expected to be present, such as in low-$E_T^{miss}$ or low-$H_T$ regions. We measure the extrapolation factor between isolated tracks and muon (electron) candidates to be $0.6\% \pm 0.2\%$ ($0.7\% \pm 0.2\%$) in a data sample dominated by Z+jets. The systematic uncertainties are assigned to be one half of the difference between the rates measured in the $\mu^+\mu^-$+ isolated track sample, and the corresponding rates measured in the $e^+e^-$+ isolated track sample since this factor should be the same for electrons and muons. The contribution of the backgrounds containing a misidentified third lepton is obtained by multiplying the number of isolated tracks in the sample with two leptons by this extrapolation factor. In a similar way we estimate the misidentified background for four-lepton events by examining two-lepton events with two isolated tracks. The rates are expected to vary with b-quark content across the control samples. The variation is accounted for by determining the rate as a function of the impact parameter distribution of non-isolated tracks in the data.

To understand the contribution from reconstructed fake hadronic taus we loosen the isolation requirements to get an extrapolation factor between loose taus and isolated taus. We extrapolate the sideband region $6\,\text{GeV} < I < 15\,\text{GeV}$ to a signal region $I < 2\,\text{GeV}$. We measure the extrapolation factor, defined as the ratio of the of number tau candidates in the signal region to the number of tau candidates in the sideband region, to be $20\% \pm 6\%$. We find that this ratio is the same for jet-triggered data and dilepton data within 30%, which is assigned as a systematic uncertainty as previously described. The ratio is applied to the $2\ell$+1 sideband tau event sample to estimate the fake hadronic-tau contribution.

## 5.3 Irreducible background from WZ and rare processes

SM processes that can produce three prompt and isolated leptons with $E_T^{miss}$ or $H_T$ are diboson+jets production where both bosons decay leptonically. This class of background is referred to as irreducible because it cannot be distinguished from the signal scenario. This irreducible background is obtained from MC simulation.

We correct the simulation to match the measured lepton efficiencies and $E_T^{miss}$ resolution. In order to correct the $E_T^{miss}$ resolution, we subdivide the $E_T^{miss}$ distribution as a function of the number of vertices and $H_T$ in the event. A large number of vertices in an event indicates a large extraneous energy in reconstructed objects due to pileup. This stochastic contribution results in poorer $E_T^{miss}$ resolution. A larger $H_T$ indicates higher jet activity, leading to systematically larger tails in the $E_T^{miss}$ distribution due to misreconstruction. We model the $E_T^{miss}$ for events without real $E_T^{miss}$ as a sum of Rayleigh distributions given by

$$p(x) = \sum_{ij} W_{ij} \frac{x}{\sigma_{ij}^2} e^{-x^2/2\sigma_{ij}^2}, \tag{1}$$

where $i$ represents the number of vertices in the event and $j$ indicates the $H_T$ bin, and the

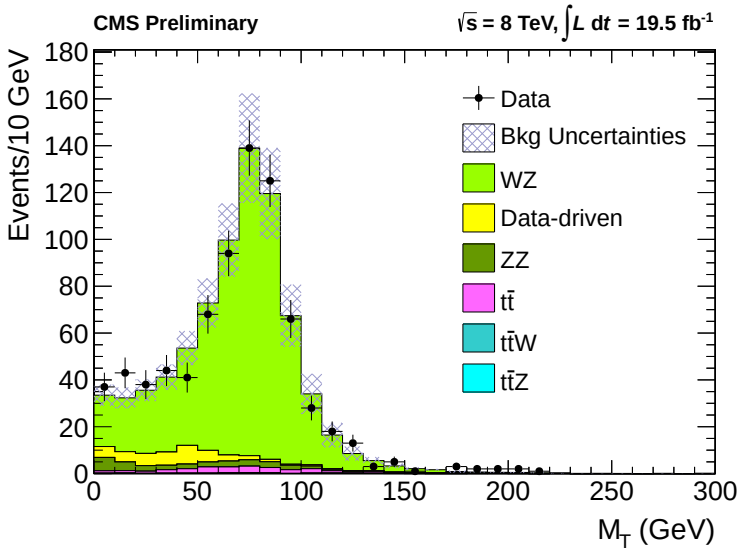


Figure 2: The transverse mass $M_{\mathrm{T}}$ distribution of events in a data sample enriched in WZ requiring an OSSF pair with $m(\ell\ell)$ in the Z-window and 50 GeV $< E_{\mathrm{T}}^{\mathrm{miss}} <$ 100 GeV.

weight $W_{ij}$ is the fraction of events in the bin. The coefficients $\sigma_{ij}$ are obtained from the fit and characterize the $E_{\mathrm{T}}^{\mathrm{miss}}$ resolution in both dilepton data and the simulation. We then vary the $E_{\mathrm{T}}^{\mathrm{miss}}$ in simulation on a per-event basis to match the coefficients with data. The magnitude of the correction to the $E_{\mathrm{T}}^{\mathrm{miss}}$ in simulation samples due to the additional variation of the $E_{\mathrm{T}}^{\mathrm{miss}}$ varies from a few percent to as high as 25%. The systematic uncertainty is obtained by studying the migration of events due to the additional $E_{\mathrm{T}}^{\mathrm{miss}}$ variation.

We verify the simulation by comparing with a data sample enriched in WZ-production, which represents the dominant contribution to trilepton signatures from diboson+jets. WZ events can be selected by requiring three leptons, 50 GeV $< E_{\mathrm{T}}^{\mathrm{miss}} <$ 100 GeV, and an on-shell Z, and $H_{\mathrm{T}} <$ 200 GeV. Figure 2 shows the observed transverse mass of the W boson. We apply a constant scale factor to the WZ simulation, chosen to normalize the simulation to data in the region 50 GeV $< M_{\mathrm{T}} <$ 120 GeV.

Our analysis also considers backgrounds from rare processes such as $\mathrm{t\bar{t}W}$, $\mathrm{t\bar{t}Z}$, $\mathrm{t\bar{b}Z}$, which we obtain from MC simulation. We use NLO cross sections of 0.2057 pb, 0.232 pb, and 0.0114 pb [24, 25], respectively, and apply a 50% systematic uncertainty on their cross sections. We also include as a background SM Higgs processes from gluon-gluon fusion, vector boson fusion, associated production with a W boson, Z boson, and top quark pair.

## 5.4 Backgrounds from asymmetric internal photon conversions

There are two different types of photon conversions that can give rise to backgrounds in multi-lepton analyses. The first type is an external conversion of an on-shell photon into an $\ell^+\ell^-$ pair in the magnetic field or material of the detector. This conversion is predominantly into $\mathrm{e^+e^-}$ pairs.

The second type is an internal conversions where the photon is off-shell and can produce muons almost as often as electrons. In the case of asymmetric conversion, where one lepton has very low $p_{\mathrm{T}}$ and does not pass the selection criteria, Drell-Yan processes with such conversions can lead to a significant background for three lepton signatures. Our lepton se-

lection strongly rejects external conversions, but the simulation of such asymmetric internal conversions is unreliable due to the soft lepton $p_T$ being below the generator-level $p_T$ thresholds. This motivates data-driven measurements of the photon to $e/\mu$ extrapolation factors as follows. We measure the conversion factors in a control region devoid of new physics (low $E_T^{miss}$ and low $H_T$). The ratio of the number of events with $|m(\ell^+\ell^-\ell'^{\pm}) - m_Z| < 15\,GeV$ or $|m(\ell^+\ell^-\ell^{\pm}) - m_Z| < 15\,GeV$ to the number of events with $|m(\ell^+\ell^-\gamma) - m_Z| < 15\,GeV$ defines the extrapolation factor, which is $0.7\% \pm 0.1\%$ ($2.1\% \pm 0.3\%$) for muons (electrons). The uncertainties are statistical only. We assign systematic uncertainties of 50% to these extrapolation factors due to our underlying assumption of proportionality between off-shell and on-shell photons. The measured extrapolation factors are then used to estimate the background in the signal regions from the observed number of $\ell^+\ell^-\gamma$ events in the search regions. The background contribution from these converted photons is small after final selections.

# 6 Results and systematic uncertainty

The expected and observed numbers of four- and three-lepton events are shown in Tables 2 and 3. The observed number of events in the channels we examine is largely consistent with expectations. Figure 3 shows a comparison of the $S_T$ distributions between data and SM predictions for some representative channels.

## 6.1 Systematic uncertainties

The sources of systematic uncertainties and how they impact the search sensitivity before extracting upper limits on the contributions from non-SM physics are discussed in this section. Sources of uncertainty related to trigger efficiencies as well as lepton identification and isolation efficiencies depend on the lepton $p_T$. The electron identification efficiency uncertainties are 14% for a $p_T$ of 10 GeV and 0.6% at 100 GeV. For muons the identification efficiency uncertainties are 11% for $p_T$ of 10 GeV and 0.2% at 100 GeV. Tau identification efficiency uncertainties are 2% for a $p_T$ of 10 GeV and 1.1% for a $p_T$ at 100 GeV.

Both signal and background estimations are subject to uncertainties on the jet energy scale, $E_T^{miss}$ resolution, luminosity, and uncertainties on the b-tagging scale factors. The luminosity uncertainty is 2.6% and only affects irreducible backgrounds and signals which are obtained from MC simulation. The uncertainty on the jet energy scale contributes 0.5% and the $E_T^{miss}$ resolution uncertainty about 4%. The effect of the uncertainties on the b-tagging scale factor is about 6%. Both background simulation and signal are also affected by theoretical uncertainties on the cross section calculations, which come from parton distribution function uncertainties and the renormalization/factorization scale uncertainties. Table 1 lists typical values for the aforementioned uncertainties.

In the case of data-driven backgrounds, the uncertainties are derived from the accuracy of the methods used to estimate these backgrounds. The overall systematic uncertainty for a channel in this search varies between 3% and 30%. WZ and ZZ simulation samples are scaled to match data in control regions. The 50% uncertainty for the $t\bar{t}$ background contribution is due to low event counts in the isolation distribution in high-$S_T$ bins, which are used to validate the misidentification rate.

| Source of Uncertainty | Uncertainty (%) |
|---|---|
| Luminosity | 2.6 |
| $E_{\mathrm{T}}^{\mathrm{miss}}$ Resolution $(0-50\ \mathrm{GeV}, 50-100\ \mathrm{GeV}, >100\ \mathrm{GeV})$ | (–3, +4, +4) |
| Jet Energy Scale WZ | 0.5 |
| b-tagging Scale Factor | 0.1 (WZ), 6 ($\mathrm{t\bar{t}}$) |
| Muon ID/Isolation at 10 (100) GeV | 11 (0.2) |
| Electron ID/Isolation at 10 (100) GeV | 14 (0.6) |
| Tau ID/isolation at 10 (100) GeV | 2 (1.1) |
| Dilepton trigger efficiency | 5 |
| $\mathrm{t\bar{t}}$ cross section | 5 |
| $\mathrm{t\bar{t}}$ fake contribution | 50 |
| WZ normalization | 6 |
| ZZ normalization | 12 |
| Asymmetric Internal conversion fake rate | 50 |
| Internal Photon Extrapolation for muons (electrons) | 0.1 (0.3) |
| Fake Muons (electrons) contribution | 0.2 (0.2) |

Table 1: The systematic uncertainties associated with this analysis.

## 6.2 Statistical procedure

We use the LandS tool to compute limits with the LHC-type CLs method [26–29]. This computation yields the observed limit as well as the expected limit with one- and two-sigma uncertainty bands. We use log-normal nuisance parameters for the signal and background uncertainties.

In order to reduce the computational resources required, a combined limit is calculated using only the channels expected to have the highest sensitivity. The channels are added in decreasing order of sensitivity until 90% of the expected signal yield is included. The discarded channels contain 10% of the signal but large SM backgrounds, so there is a large computational gain for a minimal loss of sensitivity. The expected exclusion limits obtained are consistent whether the fraction of expected signal yield included is chosen to be 90% or 95%.

For each channel, nuisance parameters are defined to describe the effect of systematic uncertainties on the signal and background yields, as well as the statistical uncertainties on both yields. While systematic uncertainties in many cases are correlated across channels, statistical uncertainties are not. Examples of nuisance parameters are the luminosity uncertainty, trigger efficiency uncertainty and others that were discussed in Section 6.1.

## 6.3 Interpretation of results

We interpret the experimental results in the context of b′ pair production with varying decay branching ratios.

Figure 4 shows the expected and observed upper limits on cross section times branching ratio for the cases $\mathcal{B}(\mathrm{b}' \to \mathrm{bZ}) = 100\%$, $\mathcal{B}(\mathrm{b}' \to \mathrm{tW}) = 100\%$, and $\mathcal{B}(\mathrm{b}' \to \mathrm{bH}) = 100\%$ with corresponding b′ masses excluded up to 520, 685, and 785 GeV.

Figure 5 shows the expected and observed limits on cross section times branching ratio for the cases $\mathcal{B}(\mathrm{b}' \to \mathrm{bH}) = 0$. As before the x-axis is the b′ mass, the y-axis is $\mathcal{B}(\mathrm{b}' \to \mathrm{bZ})$ and all points to the left of the curve are excluded.

4

| $N_{OSSF}$ | on- or off-Z | $S_T$ (TeV) | $N_{\tau_h} = 0, N_{b\text{-jets}} = 0$ obs | exp | $N_{\tau_h} \geq 1, N_{b\text{-jets}} = 0$ obs | exp | $N_{\tau_h} = 0, N_{b\text{-jets}} \geq 1$ obs | exp | $N_{\tau_h} \geq 1, N_{b\text{-jets}} \geq 1$ obs | exp |
|---|---|---|---|---|---|---|---|---|---|---|
| 0 | - | $> 2.0$ | 0 | $< 0.02$ | 0 | $0 \pm 0.02$ | 0 | $0 \pm 0.02$ | 0 | $0 \pm 0.02$ |
| 0 | - | $1.5 - 2.0$ | 0 | $< 0.02$ | 0 | $0 \pm 0.02$ | 0 | $0 \pm 0.02$ | 0 | $0 \pm 0.02$ |
| 0 | - | $1.0 - 1.5$ | 0 | $< 0.02$ | 0 | $0 \pm 0.02$ | 0 | $0 \pm 0.02$ | 0 | $0.007 \pm 0.02$ |
| 0 | - | $0.6 - 1.0$ | 0 | $< 0.02$ | 0 | $0.12 \pm 0.11$ | 0 | $0.05 \pm 0.05$ | †0 | $0.12 \pm 0.1$ |
| 0 | - | $0.3 - 0.6$ | 0 | $0.09 \pm 0.06$ | 1 | $0.5 \pm 0.19$ | 0 | $0.001 \pm 0.02$ | 0 | $0.28 \pm 0.12$ |
| 0 | - | $0 - 0.3$ | 0 | $0.05 \pm 0.05$ | 2 | $1.1 \pm 0.45$ | 0 | $0.0003 \pm 0.02$ | 0 | $0.25 \pm 0.16$ |
| 1 | offZ | $> 2.0$ | 0 | $< 0.02$ | 0 | $0 \pm 0.02$ | 0 | $0 \pm 0.02$ | 0 | $0 \pm 0.02$ |
| 1 | onZ | $> 2.0$ | 0 | $< 0.02$ | 0 | $0 \pm 0.02$ | 0 | $0 \pm 0.02$ | 0 | $0 \pm 0.02$ |
| 1 | offZ | $1.5 - 2.0$ | 0 | $< 0.02$ | 0 | $0.007 \pm 0.02$ | 0 | $0 \pm 0.02$ | 0 | $0 \pm 0.02$ |
| 1 | onZ | $1.5 - 2.0$ | 0 | $< 0.02$ | 0 | $0.02 \pm 0.03$ | 0 | $0.01 \pm 0.03$ | 0 | $0.007 \pm 0.02$ |
| 1 | offZ | $1.0 - 1.5$ | 0 | $0.002 \pm 0.02$ | 0 | $0.12 \pm 0.07$ | †0 | $0.03 \pm 0.04$ | 0 | $0.02 \pm 0.02$ |
| 1 | onZ | $1.0 - 1.5$ | 1 | $0.06 \pm 0.06$ | 0 | $0.1 \pm 0.07$ | 0 | $0.11 \pm 0.08$ | 0 | $0.04 \pm 0.04$ |
| 1 | offZ | $0.6 - 1.0$ | 0 | $0.06 \pm 0.04$ | 2 | $0.48 \pm 0.17$ | 0 | $0.06 \pm 0.07$ | †0 | $0.3 \pm 0.13$ |
| 1 | onZ | $0.6 - 1.0$ | 0 | $0.43 \pm 0.15$ | 0 | $1.7 \pm 0.6$ | 0 | $0.5 \pm 0.29$ | †0 | $0.7 \pm 0.33$ |
| 1 | offZ | $0.3 - 0.6$ | 0 | $0.27 \pm 0.11$ | 4 | $2.1 \pm 0.5$ | 0 | $0.33 \pm 0.17$ | 0 | $1.2 \pm 0.43$ |
| 1 | onZ | $0.3 - 0.6$ | 5 | $1.8 \pm 0.47$ | 10 | $12 \pm 3$ | 2 | $1 \pm 0.5$ | 2 | $1.6 \pm 0.5$ |
| 1 | offZ | $0 - 0.3$ | 2 | $0.48 \pm 0.18$ | 18 | $8.3 \pm 2.1$ | 0 | $0.04 \pm 0.04$ | 1 | $0.6 \pm 0.3$ |
| 1 | onZ | $0 - 0.3$ | 2 | $3 \pm 0.9$ | 43 | $41 \pm 10$ | 2 | $0.07 \pm 0.04$ | 2 | $1 \pm 0.4$ |
| 2 | offZ | $> 2.0$ | 0 | 1e-05 $\pm$ 0.02 | - | - | 0 | $0 \pm 0.02$ | - | - |
| 2 | onZ | $> 2.0$ | 0 | $0.002 \pm 0.02$ | - | - | 0 | $0.02 \pm 0.03$ | - | - |
| 2 | offZ | $1.5 - 2.0$ | 0 | $0.0002 \pm 0.02$ | - | - | 0 | $0 \pm 0.02$ | - | - |
| 2 | onZ | $1.5 - 2.0$ | 0 | $0.05 \pm 0.03$ | - | - | 0 | $0.01 \pm 0.02$ | - | - |
| 2 | offZ | $1.0 - 1.5$ | 0 | $0.01 \pm 0.02$ | - | - | 0 | $0 \pm 0.02$ | - | - |
| 2 | onZ | $1.0 - 1.5$ | 1 | $0.6 \pm 0.26$ | - | - | †0 | $0.1 \pm 0.05$ | - | - |
| 2 | offZ | $0.6 - 1.0$ | 0 | $0.11 \pm 0.04$ | - | - | 0 | $0.14 \pm 0.08$ | - | - |
| 2 | onZ | $0.6 - 1.0$ | 4 | $5.9 \pm 2.0$ | - | - | 1 | $1 \pm 0.39$ | - | - |
| 2 | offZ | $0.3 - 0.6$ | 3 | $1 \pm 0.3$ | - | - | 1 | $0.22 \pm 0.1$ | - | - |
| 2 | onZ | $0.3 - 0.6$ | 26 | $42 \pm 10$ | - | - | 4 | $3.2 \pm 1$ | - | - |
| 2 | offZ | $0 - 0.3$ | 7 | $8.2 \pm 2.3$ | - | - | 0 | $0.18 \pm 0.07$ | - | - |
| 2 | onZ | $0 - 0.3$ | *135 | $122 \pm 29$ | - | - | 1 | $1 \pm 0.26$ | - | - |
| Total4 | All | All | 186 | $187 \pm 39$ | 80 | $68 \pm 15$ | 11 | $8.3 \pm 2.7$ | 5 | $6.3 \pm 1.6$ |

Table 2: Observed yields for four lepton events from 19.5 $fb^{-1}$ recorded in 2012. The channels are broken down by the number of and mass of any opposite-sign same-flavor pairs (whether on or off Z), whether the leptons include taus, whether there are any b jets present and the $S_T$. Expected yields are the sum of simulation and data-driven estimates of backgrounds in each channel. The channels are exclusive. Channels marked with an asterisk are used as control regions and are excluded from the limit calculations. Also, those channels with a dagger mark are used in the limit setting procedure and are representative of the top most sensitive channels for the $b'$ decay with mass of 500 GeV where $\mathcal{B}(b' \to bH) = 1.0$.

The expected exclusion curve in Figure 5 can be estimated from the branching ratios of a b′ pair to decay into three and four leptons, as a function of B(b′→ bZ). Defining $\alpha \equiv$ B(b′→ bZ) and assuming B(b′→ bH) to be 0, the the different branching ratios of a b′ pair decay can be written as bZbZ $= \alpha^2$, bZtW $= 2\alpha$(1-$\alpha$), and tWtW $= (1-\alpha)^2$, respectively. The branching ratio of B( b′b′ →≥ 3 leptons) is then given by:

$$f(\alpha) = (0.36\%)\alpha^2 + (2.65\%)2\alpha(1-\alpha) + (5.1\%)(1-\alpha)^2 \quad (2)$$

The first coefficient 0.36% corresponds to the branching ratio of bZbZ into four leptons, and 2.65%, and 5.1% correspond to the branching ratios of bZtW and tWtW into three or more leptons. Equation 2 exhibits a quadratic dependence on $\alpha$, and the mass limit is expected to improve as $\alpha$ decreases.

Figure 6 shows the benchmark branching ratio $\mathcal{B}(b' \to tW) = 50\%$, $\mathcal{B}(b' \to bH) = 25\%$, and $\mathcal{B}(b' \to bZ) = 25\%$ for which we calculate an exclusion limit of 694 GeV for the mass of the vector-like b′ quark.

Figure 7 shows the expected and observed curves respectively as a function of the branching ratios to $b' \to bZ$, $b' \to tW$, and $b' \to bH$. The x-axis is the b′ mass and the y-axis is $\mathcal{B}(b' \to bZ)$. The different contours are curves of fixed BR($b' \to bH$) and all points to the left of a given curve

| $N_{OSSF}$ | $m(\ell^+\ell^-)$ (GeV) | $S_T$ (TeV) | $N_{\tau_h}=0, N_{\text{b-jets}}=0$ obs | exp | $N_{\tau_h}=1, N_{\text{b-jets}}=0$ obs | exp | $N_{\tau_h}=0, N_{\text{b-jets}}\geq 1$ obs | exp | $N_{\tau_h}=1, N_{\text{b-jets}}\geq 1$ obs | exp |
|---|---|---|---|---|---|---|---|---|---|---|
| 0 | - | $> 2.0$ | 0 | $< 0.02$ | 0 | $0.04 \pm 0.05$ | 0 | $0 \pm 0.02$ | 0 | $0 \pm 0.22$ |
| 0 | - | $1.5 - 2.0$ | 0 | $0.07 \pm 0.06$ | 0 | $0.18 \pm 0.19$ | 0 | $0.05 \pm 0.06$ | 0 | $0.46 \pm 0.28$ |
| 0 | - | $1.0 - 1.5$ | 0 | $0.21 \pm 0.18$ | 2 | $2.6 \pm 1.2$ | 0 | $0.36 \pm 0.14$ | 2 | $3.9 \pm 2$ |
| 0 | - | $0.6 - 1.0$ | †3 | $3.1 \pm 1$ | †26 | $28 \pm 12$ | 2 | $4.9 \pm 1.9$ | †46 | $58 \pm 28$ |
| 0 | - | $0.3 - 0.6$ | 32 | $27 \pm 10$ | 289 | $290 \pm 129$ | 42 | $39 \pm 17$ | 410 | $480 \pm 241$ |
| 0 | - | $0 - 0.3$ | 72 | $79 \pm 22$ | 1194 | $1324 \pm 330$ | 37 | $32 \pm 15$ | 316 | $331 \pm 160$ |
| 1 | $> 105$ | $> 2.0$ | 0 | $0.001 \pm 0.02$ | 0 | $0 \pm 0.21$ | 0 | $0 \pm 0.03$ | 0 | $0 \pm 0.21$ |
| 1 | $< 75$ | $> 2.0$ | 0 | $0.004 \pm 0.02$ | 0 | $0 \pm 0.21$ | 0 | $0.01 \pm 0.04$ | 0 | $0 \pm 0.21$ |
| 1 | onZ | $> 2.0$ | 0 | $0.2 \pm 0.12$ | 0 | $0.009 \pm 0.21$ | 0 | $0.04 \pm 0.06$ | 0 | $0.04 \pm 0.05$ |
| 1 | $> 105$ | $1.5 - 2.0$ | 0 | $0.15 \pm 0.09$ | 0 | $0.22 \pm 0.22$ | 0 | $0.08 \pm 0.05$ | 0 | $0.2 \pm 0.18$ |
| 1 | $< 75$ | $1.5 - 2.0$ | 1 | $0.11 \pm 0.08$ | 0 | $0.03 \pm 0.05$ | 0 | $0.07 \pm 0.05$ | 0 | $0.06 \pm 0.07$ |
| 1 | onZ | $1.5 - 2.0$ | 3 | $1.1 \pm 0.6$ | 0 | $0.31 \pm 0.17$ | 1 | $0.28 \pm 0.18$ | 0 | $0.25 \pm 0.12$ |
| 1 | $> 105$ | $1.0 - 1.5$ | 2 | $1 \pm 0.4$ | 1 | $1.3 \pm 0.6$ | 0 | $0.5 \pm 0.22$ | 1 | $2.1 \pm 1.2$ |
| 1 | $< 75$ | $1.0 - 1.5$ | 0 | $1.1 \pm 0.38$ | 1 | $0.9 \pm 0.44$ | †1 | $0.6 \pm 0.27$ | 0 | $1 \pm 0.7$ |
| 1 | onZ | $1.0 - 1.5$ | 11 | $15 \pm 6.9$ | 9 | $5.9 \pm 1.6$ | 2 | $3.3 \pm 1.2$ | 1 | $1.7 \pm 0.6$ |
| 1 | $> 105$ | $0.6 - 1.0$ | 13 | $10 \pm 2.4$ | 21 | $23 \pm 7.2$ | †7 | $7.4 \pm 2.4$ | 23 | $28 \pm 14$ |
| 1 | $< 75$ | $0.6 - 1.0$ | 14 | $10 \pm 3.6$ | 21 | $11 \pm 3.4$ | †4 | $8.3 \pm 2.6$ | †14 | $12 \pm 6$ |
| 1 | onZ | $0.6 - 1.0$ | 106 | $111 \pm 40$ | 108 | $70 \pm 17$ | †16 | $24 \pm 7$ | 17 | $17 \pm 4.7$ |
| 1 | $> 105$ | $0.3 - 0.6$ | 63 | $65 \pm 12$ | 285 | $372 \pm 96$ | 36 | $35 \pm 13$ | 169 | $187 \pm 94$ |
| 1 | $< 75$ | $0.3 - 0.6$ | 84 | $86 \pm 21$ | 290 | $279 \pm 71$ | 52 | $56 \pm 22$ | 167 | $171 \pm 87$ |
| 1 | onZ | $0.3 - 0.6$ | *669 | $735 \pm 166$ | *2099 | $2705 \pm 772$ | 122 | $108 \pm 24$ | 325 | $284 \pm 73$ |
| 1 | $> 105$ | $0 - 0.3$ | 180 | $195 \pm 33$ | 1620 | $1712 \pm 482$ | 17 | $17 \pm 6.4$ | 97 | $79 \pm 35$ |
| 1 | $< 75$ | $0 - 0.3$ | 617 | $644 \pm 102$ | 10173 | $9211 \pm 2694$ | 62 | $74 \pm 28$ | 297 | $288 \pm 97$ |
| 1 | onZ | $0 - 0.3$ | *4255 | $4439 \pm 691$ | *49916 | $49192 \pm 14670$ | *140 | $149 \pm 24$ | 795 | $826 \pm 229$ |
| Total3 | All | All | 6125 | $6430 \pm 916$ | 66055 | $65233 \pm 19038$ | 541 | $564 \pm 150$ | 2680 | $2774 \pm 903$ |

Table 3: Observed yields for three lepton events. The channels are broken down by the number of and mass of any opposite-sign, same-flavor pairs (whether on or off Z), whether the leptons include taus, whether there are any b jets present and the $S_T$. Expected yields are the sum of simulation and data-driven estimates of backgrounds in each channel. The channels are exclusive. Channels marked with an asterisk are used as control regions and are excluded from the limit calculations. Also, those channels marked with a dagger are a representative subset of the top most sensitive channels for the $b'$ decay, with a mass of 500 GeV and $\mathcal{B}(\text{b}' \to \text{bH}) = 1.0$, which are used in the limit setting procedure.

are excluded at the 95% confidence level. As $\mathcal{B}(\text{b}' \to \text{bH})$ increases, the total acceptance into 3- and 4-lepton decreases which results in less sensitivity.

The full interpretation of the results taking into account all combinations of the various branching ratios is shown in Figure 8. Table 4 shows the observed and expected limits at 95% CL for a few of these branching ratio combinations.

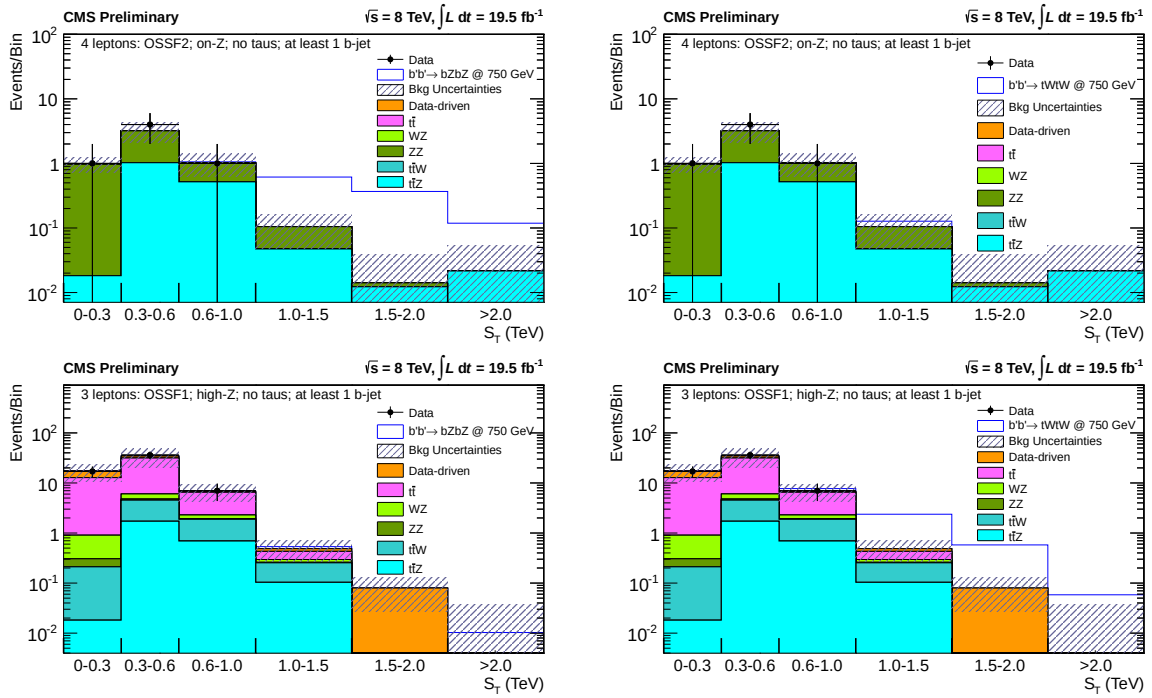


Figure 3: $S_{\mathrm{T}}$ distributions for channels with expected signal overlaid. The left column contains $\mathrm{b'b'} \to \mathrm{bZbZ}$ as the signal and the right column contains $\mathrm{b'b'} \to \mathrm{tWtW}$ as the signal with b′ having a mass of 750 GeV. The top row is the channel with 4 leptons, such that they form 2 opposite-sign same-flavor pairs where at least one of of them is on-Z and none of them are taus with at least 1 b jet. The bottom row is the channel with 3 leptons, such that they form 1 opposite-sign same-flavor pair having invariant mass above the Z-window and none of them are taus, and at least 1 b jet. Channels marked with an asterisk are used as control regions and are excluded from the limit calculations. Also, those channels marked with a dagger are a representative subset of the top most sensitive channels for the $b'$ decay, with a mass of 500 GeV and $\mathcal{B}(\mathrm{b'} \to \mathrm{bH}) = 1.0$, which are used in the limit setting procedure.

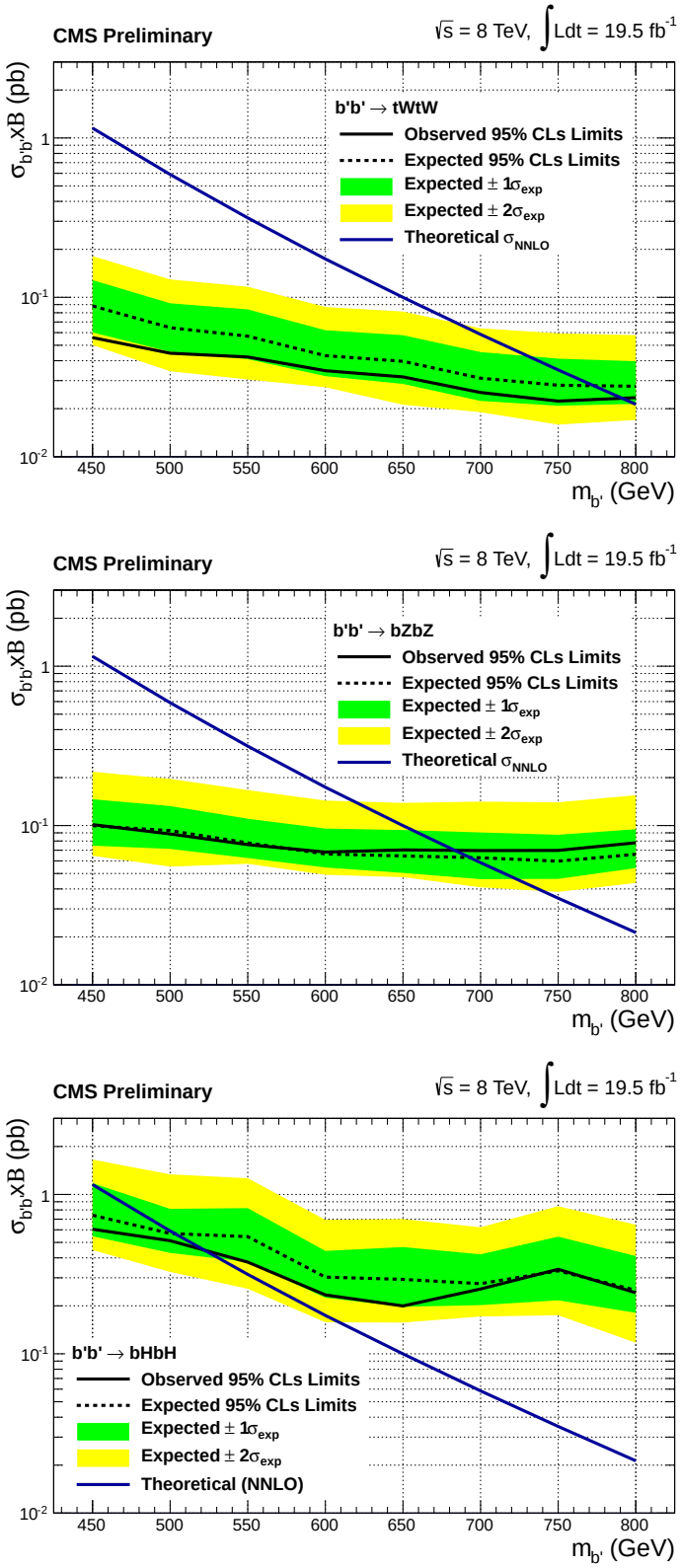


Figure 4: Cross section times branching ratio exclusion curves for a b′ as a function of its mass for the decay modes b′b′ → tWtW (top), b′b′ → bZbZ (middle), and b′b′ → bHbH (bottom). The figures show expected (dashed), observed (solid) exclusions; sigma bands correspond to the experimental uncertainties

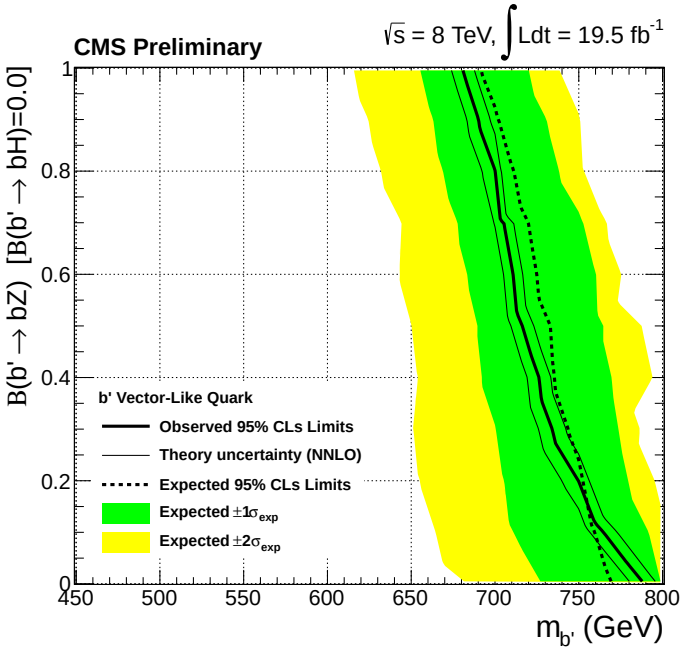


Figure 5: Exclusion limits for pair-produced b′ quarks going to multileptons in the two-dimensional plane of branching ratio of b′ to bZ vs. b′ mass. Signal points to the left of the curve are excluded. The y = 0 axis corresponds to b′b′ → tWtW and the $y = 1$ axis to b′b′ → bZbZ. The branching ratio for b′ → bH is set to zero. We apply a conservative 10% theory uncertainty.

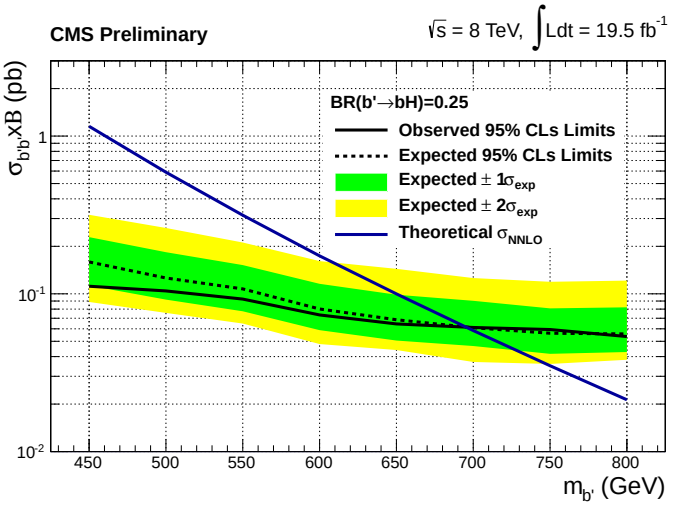


Figure 6: Observed and expected 95% confidence level upper limits for the b′ quark production cross section for branching ratio into into tW, bH, and bZ of 50%, 25%, and 25%, respectively.

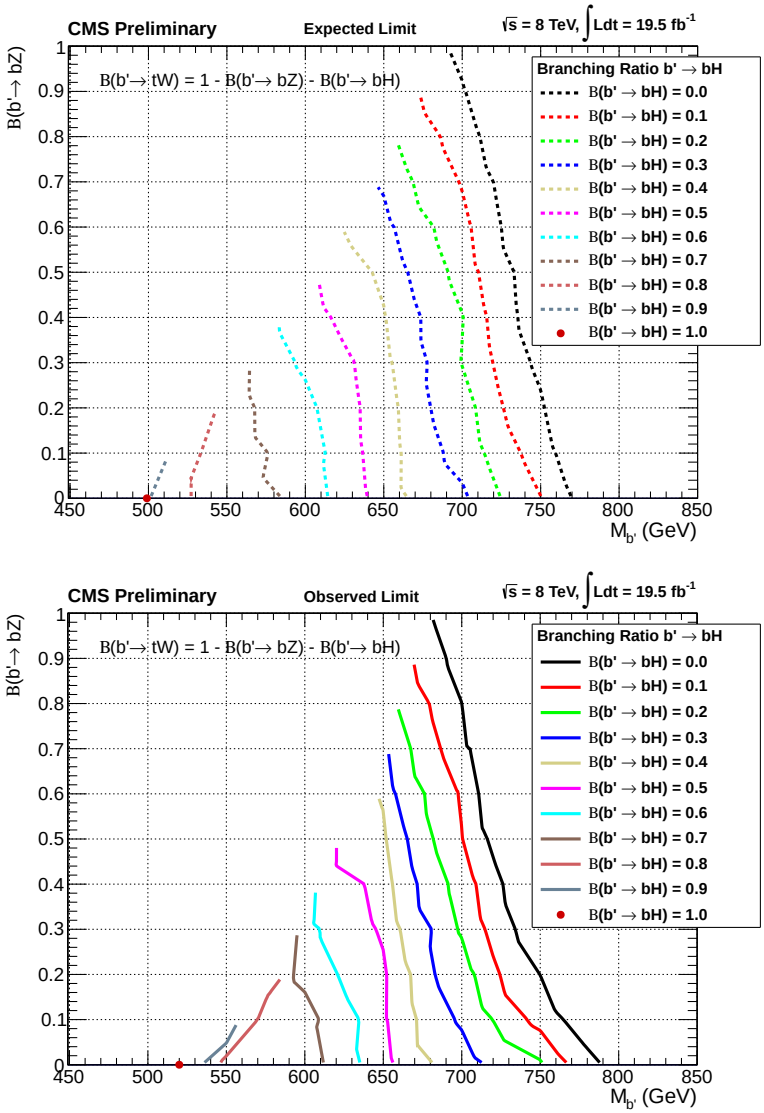


Figure 7: Expected (top) and observed (bottom) exclusion curves as a function of branching ratios. The $\mathcal{B}(\mathrm{b}' \to \mathrm{bZ})$ is plotted as a function of the b′ mass and the various curves represent fixed $\mathcal{B}(\mathrm{b}' \to \mathrm{bH})$ from 0.0 (the rightmost) to 1.0 ( the leftmost)

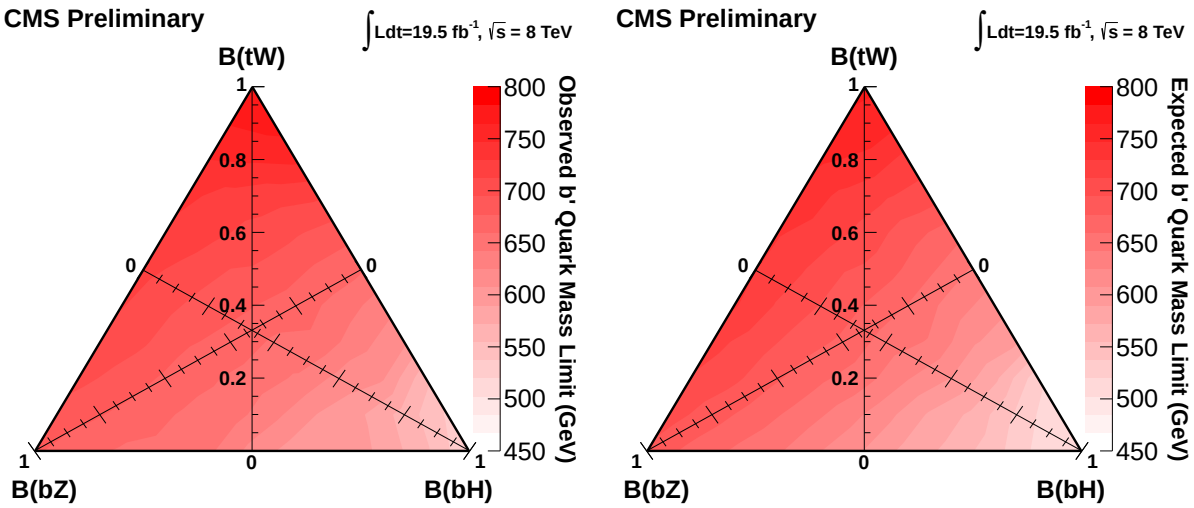


Figure 8: Expected and observed limit results with varied branching ratio of tW, bH, and bZ in steps of 0.1.

| Comb # | $\mathcal{B}$(H→tW) | $\mathcal{B}$(H→bH) | $\mathcal{B}$(H→bZ) | obs (GeV) | exp (GeV) | $\pm1\sigma$ (GeV) | $\pm2\sigma$ (GeV) |
|---|---|---|---|---|---|---|---|
| (0) | 0.5 | 0.3 | 0.3 | 694 | 692 | [651,723] | [605,759] |
| (1) | 0.0 | 0.0 | 1.0 | 680 | 691 | [655,719] | [617,750] |
| (2) | 0.0 | 0.1 | 0.9 | 666 | 672 | [637,707] | [600,711] |
| (3) | 0.0 | 0.2 | 0.8 | 657 | 657 | [616,685] | [578,708] |
| (4) | 0.0 | 0.3 | 0.7 | 654 | 645 | [596,668] | [561,672] |
| (5) | 0.0 | 0.4 | 0.6 | 646 | 625 | [578,657] | [542,672] |
| (6) | 0.0 | 0.5 | 0.5 | 618 | 606 | [564,643] | [517,648] |
| (7) | 0.0 | 0.6 | 0.4 | 598 | 583 | [547,620] | [501,639] |
| (8) | 0.0 | 0.7 | 0.3 | 605 | 566 | [519,613] | [474,631] |
| (9) | 0.0 | 0.8 | 0.2 | 584 | 543 | [501,593] | [457,628] |
| (10) | 0.0 | 0.9 | 0.1 | 557 | 514 | [466,546] | [438,627] |
| (11) | 0.0 | 1.0 | 0.0 | 520 | 502 | [447,528] | [423,607] |
| (12) | 0.1 | 0.0 | 0.9 | 688 | 703 | [661,724] | [622,742] |
| (13) | 0.1 | 0.1 | 0.8 | 678 | 686 | [649,716] | [607,717] |
| (14) | 0.1 | 0.2 | 0.7 | 667 | 669 | [629,701] | [589,725] |
| (15) | 0.1 | 0.3 | 0.6 | 657 | 653 | [610,682] | [567,709] |
| (16) | 0.1 | 0.4 | 0.5 | 650 | 635 | [589,665] | [547,700] |
| (17) | 0.1 | 0.5 | 0.4 | 629 | 613 | [567,652] | [525,665] |
| (18) | 0.1 | 0.6 | 0.3 | 606 | 587 | [546,645] | [499,659] |
| (19) | 0.1 | 0.7 | 0.2 | 592 | 568 | [516,615] | [474,651] |
| (20) | 0.1 | 0.8 | 0.1 | 565 | 533 | [484,595] | [451,632] |
| (21) | 0.1 | 0.9 | 0.0 | 534 | 503 | [458,543] | [436,587] |

Table 4: Sets of branching ratio values and the observed and expected 95% CL upper limits for the combined electron and muon channels.

# 7 Conclusion

We have performed a search for pair-production of vector-like partners of the b quark, b′, with multilepton final states using 19.5 fb$^{-1}$ of integrated luminosity in pp collisions at $\sqrt{s} = 8$ TeV. We binned the data in several exclusive channels according to the amount of expected standard model background in order to increase the search sensitivity. We see good agreement between observations and expectations. The search is interpreted for different b′ mass and for varying branching ratios to the bZ, tW, and bH states. We exclude b′ quarks with masses less than values in the range 520-785 GeV (depending on the values of the branching ratios) at the 95% confidence level.

# References

[1] CMS Collaboration, "Observation of a new boson at a mass of 125 GeV with the CMS experiment at the LHC", *Phys. Lett. B* **716** (2012) 30–61, doi:10.1016/j.physletb.2012.08.021, arXiv:1207.7235.

[2] P. H. Frampton, P. Hung, and M. Sher, "Quarks and leptons beyond the third generation", *Phys. Rept.* **330** (2000) 263, doi:10.1016/S0370-1573(99)00095-2, arXiv:hep-ph/9903387.

[3] M. Schmaltz and D. Tucker-Smith, "Little Higgs review", *Ann. Rev. Nucl. Part. Sci.* **55** (2005) 229–270, doi:10.1146/annurev.nucl.55.090704.151502, arXiv:hep-ph/0502182.

[4] N. Arkani-Hamed, A. G. Cohen, and H. Georgi, "Electroweak symmetry breaking from dimensional deconstruction", *Phys. Lett. B* **513** (2001) 232–240, doi:10.1016/S0370-2693(01)00741-9, arXiv:hep-ph/0105239.

[5] CMS Collaboration, "Combined search for the quarks of a sequential fourth generation", *Phys.Rev. D* **86** (2012) 112003, doi:10.1103/PhysRevD.86.112003, arXiv:1209.1062.

[6] B. A. Dobrescu, K. Kong, and R. Mahbubani, "Prospects for top-prime quark discovery at the Tevatron", *JHEP* **0906** (2009) 001, doi:10.1088/1126-6708/2009/06/001, arXiv:0902.0792.

[7] M. Sher, "Fourth Generation $b'$ decays into b + Higgs", arXiv:9908238v2.

[8] The LHC Higgs Cross Section Working Group Collaboration, "Handbook of LHC Higgs Cross Sections: 3. Higgs Properties", arXiv:1307.1347.

[9] GEANT4 Collaboration, "GEANT4: A simulation toolkit", *Nucl. Instrum. Meth. A* **506** (2003) 250, doi:10.1016/S0168-9002(03)01368-8.

[10] J. Alwall et al., "MADGRAPH 5: Going Beyond", *JHEP* **1106** (2011) 128, doi:10.1007/JHEP06(2011)128, arXiv:1106.0522.

[11] F. Maltoni and T. Stelzer, "MadEvent: Automatic event generation with MadGraph", *JHEP* **02** (2003) 027, doi:10.1088/1126-6708/2003/02/027.

[12] P. M. Nadolsky et al., "Implications of CTEQ global analysis for collider observables", *Phys. Rev. D* **78** (2008) 013004, doi:10.1103/PhysRevD.78.013004, arXiv:0802.0007.

[13] M. Czakon, P. Fiedler, and A. Mitov, "The total top quark pair production cross-section at hadron colliders through $O(\alpha_S^4)$", *Phys.Rev.Lett.* **110** (2013) 252004, doi:10.1103/PhysRevLett.110.252004, arXiv:1303.6254.

[14] CMS Collaboration, "Commissioning of the Particle-Flow Reconstruction in Minimum-Bias and Jet Events from pp Collisions at 7 TeV", *CMS Physics Analysis Summary* **CMS-PAS-PFT-10-002** (2010).

[15] CMS Collaboration, "Performance of muon identification in pp collisions at $\sqrt{s}$ = 7 TeV", *CMS Physics Analysis Summary* **CMS-PAS-MUO-10-002** (2010).

[16] CMS Collaboration, "Electron Reconstruction and Identification at $\sqrt{s} = 7$ TeV", *CMS Physics Analysis Summary* **CMS-PAS-EGM-10-004** (2010).

[17] CMS Collaboration, "Performance of $\tau$-lepton reconstruction and identification in CMS", *JINST* **7** (2012), no. 01, P01001.

[18] M. Cacciari, G. Salam, and G. Soyez, "The Anti-$k_T$ Jet Clustering Algorithm", *JHEP* **04** (2008) 063, doi:10.1088/1126-6708/2008/04/063.

[19] G. Soyez et al., "Pileup subtraction for jet shapes", *Phys.Rev.Lett.* **110** (2013) 162001, doi:10.1103/PhysRevLett.110.162001, arXiv:1211.2811.

[20] CMS Collaboration, "Pileup measurement and mitigation techniques in CMS", *J.Phys.Conf.Ser.* **404** (2012) 012045, doi:10.1088/1742-6596/404/1/012045.

[21] CMS Collaboration, "Identification of b-quark jets with the CMS experiment", *JINST* **8** (2013) P04013, doi:10.1088/1748-0221/8/04/P04013, arXiv:1211.4462.

[22] CMS Collaboration, "Missing Transverse Energy Performance in Minimum-Bias and Jet Events from Proton-Proton Collisions at $\sqrt{s} = 7$ TeV", *CMS Physics Analysis Summary* **CMS-PAS-JME-10-004** (2010).

[23] CMS Collaboration, "CMS MET Performance in Events Containing Electroweak Bosons from pp Collisions at $\sqrt{s} = 7$ TeV", *CMS Physics Analysis Summary* **CMS-PAS-JME-10-005** (2010).

[24] J. M. Campbell and R. K. Ellis, "$t\bar{t}W^{+-}$ production and decay at NLO", *JHEP* **1207** (2012) 052, doi:10.1007/JHEP07(2012)052, arXiv:1204.5678.

[25] M. Garzelli, A. Kardos, C. Papadopoulos, and Z. Trocsanyi, "t $\bar{t}$ $W^{+-}$ and t $\bar{t}$ Z Hadroproduction at NLO accuracy in QCD with Parton Shower and Hadronization effects", *JHEP* **1211** (2012) 056, doi:10.1007/JHEP11(2012)056, arXiv:1208.2665.

[26] CMS Collaboration, "Procedure for the LHC Higgs boson search combination in summer 2011", Technical Report ATL-PHYS-PUB-2011-011, CERN, Geneva, (Aug, 2011).

[27] Mingshui Chen et al, "LandS software package". http://cern.ch/mschen/LandS, 2013.

[28] T. Junk, "Confidence Level Computation for Combining Searches with Small Statistics", *Nucl. Instrum. Meth. A* **434** (1999) 435–443, doi:10.1016/S0168-9002(99)00498-2, arXiv:hep-ex/9902006.

[29] A. L. Read, "Presentation of search results: The CL(s) technique", *J. Phys. G* **28** (2002) 2693–2704, doi:10.1088/0954-3899/28/10/313.